Optics Letters

Airborne temperature profiling in the troposphere during daytime by lidar utilizing Rayleigh–Brillouin scattering

Benjamin Witschas,* Christian Lemmerz, Oliver Lux, Uwe Marksteiner, Oliver Reitebuch, and Andreas Schäfler

Deutsches Zentrum für Luft- und Raumfahrt e.V. (DLR), Institut für Physik der Atmosphäre, 82234 Oberpfaffenhofen, Germany
**Corresponding author: Benjamin.Witschas@dlr.de*

Received 12 May 2021; revised 2 July 2021; accepted 9 July 2021; posted 9 July 2021 (Doc. ID 431350); published 19 August 2021

The airborne measurement of a temperature profile from 10.5 km down towards ground (≈1.4 km above sea level) during daytime by means of a lidar utilizing Rayleigh–Brillouin (RB) scattering is demonstrated for the first time, to our knowledge. The spectra of the scattered light were measured by tuning the laser ($\lambda = 354.9$ nm) over a 11 GHz frequency range with a step size of 250 MHz while using a Fabry–Perot interferometer as a spectral filter. The measurement took 14 min and was conducted over a remote area in Iceland with the ALADIN Airborne Demonstrator on-board the DLR Falcon aircraft. The temperature profile was derived by applying an analytical RB line shape model to the backscatter spectra, which were measured at different altitudes with a vertical resolution of 630 m. A comparison with temperature profiles from radiosonde observations and model temperatures shows reasonable agreement with biases of less than ±2 K. Based on Poisson statistics, the random error of the derived temperatures is estimated to vary between 0.1 K and 0.4 K. The work provides insight into the possible realization of airborne lidar temperature profilers based on RB scattering.

https://doi.org/10.1364/OL.431350

Temperature is a fundamental quantity that is needed to describe the state of the atmosphere. Thus, observational data of temperature profiles are important inputs to numerical weather prediction and for data retrievals of other atmospheric quantities such as wind and relative humidity. Therefore, various *in situ* and remote sensing technologies have been developed to provide spatially and temporally resolved temperature profiles [1].

A successful active remote sensing method is lidar, which can be used to acquire temperature profiles from ground up to the mesosphere (≈105 km) with adequate accuracy (≈1 K) and high temporal (≈ a few minutes) and vertical resolution (≈100 m) [2]. For tropospheric temperature profiling with lidar, it is common to make use of rotational Raman scattering on air molecules [3,4], although powerful lasers and long integration times are needed due to the small Raman scattering cross section. An alternative method is the usage of high spectral resolution lidars (HSRLs), which infer temperature from the shape of the Rayleigh–Brillouin (RB) spectrum. Due to the larger Rayleigh scattering cross section and the smaller spectral extent compared to Raman scattering, HSRL measurements can be performed with low-power lasers, smaller telescopes, and during daytime [5,6]. Usually, HSRL systems use atomic vapor cells [7–9] or interferometers [5] to separate the molecular from the aerosol signal and apply a RB line shape model for temperature retrieval. A modified approach was introduced by Witschas *et al.* [6] who resolved the entire RB spectrum by tuning the laser over a 12 GHz frequency range and using a Fabry–Perot interferometer (FPI) as a spectral filter. With this, tropospheric temperature profiles were measured from 2 km to 15 km with a vertical resolution of 0.3 km to 2.2 km and showed differences to radiosonde temperatures of <2.5 K in cloud-free conditions. Recently, Stillwell *et al.* [10] demonstrated temperature measurements during day and nighttime from ground up to 4 km with a vertical and temporal resolution of 225 m and 30 min and with an accuracy of better than 3 K, by applying the differential absorption lidar technique. This reveals that different tropospheric temperature sounding techniques have been demonstrated by ground-based lidars. However, measurements from airborne platforms that can provide data at times and locations that are inaccessible for ground-based systems are still rare.

To this day, results of only a few airborne temperature lidar systems have been published. Airborne measurements of tropospheric temperatures are all based on Raman scattering, whereas temperature profiles in the stratosphere have been measured by means of Rayleigh scattering [11,12]. Advantageously, as no aerosols are usually present in the middle and upper stratosphere, the number of backscattered photons can be related to the molecular number density and hence to atmospheric temperature. However, this approach does not work in the troposphere, where aerosols are mostly present. In 1996, Heaps *et al.* [13] reported on airborne Raman lidar measurements performed from 6 km altitude, but did not discuss results of temperature measurements. Later, in 2002, Burris *et al.* [14]

showed measurements of their upwards measuring airborne Rayleigh/Raman lidar providing temperature profiles from flight level (≈11 km) up to 60 km. Comparisons to radiosonde and *in situ* measurements showed excellent agreement with systematic and random errors of about 1 K. In 2016, Wu *et al.* [15] demonstrated airborne temperature measurements in the troposphere during nighttime by means of a compact rotational Raman lidar from flight level (≈3 km) down to ground. The random error was determined to be always better than 3 K. Lately, Rehky *et al.* [16] published a feasibility study regarding the opportunity of using filtered Rayleigh scattering to measure temperature and density profiles below a supersonic aircraft; however, no information about the accuracy of these measurements is estimated.

In this Letter, we report on the first tropospheric temperature profile measurement during daytime from a flight altitude of 11 km down towards the ground by means of a lidar utilizing RB scattering. The instrumental architecture and the applied measurement principle are explained in detail by Witschas *et al.* [6] based on ground-based measurements. Here, the method was applied to a temperature profile measurement in flight to demonstrate its feasibility even in the harsh environment of an airborne platform and particularly at daylight conditions as well as in a region that is difficult to access from ground.

During the North Atlantic Waveguide and Downstream Impact Experiment (NAWDEX), conducted in Sep/Oct 2016 [17] from Keflavik, Iceland, the German Aerospace Center (Deutsches Zentrum für Luft- und Raumfahrt, DLR) deployed two airborne wind lidar systems aboard their Falcon aircraft [18]. Besides providing accurate wind speed measurements of the North Atlantic jet stream, another goal was the preparation of the first spaceborne wind lidar mission, Aeolus, launched on August 22, 2018, by the European Space Agency. The DLR Falcon aircraft was equipped with a prototype of the Aeolus satellite instrument, the ALADIN Airborne Demonstrator (A2D) [19,20], as well as with a coherent detection wind lidar used as a reference instrument [21]. The same payload was used in later campaigns after launch to validate the Aeolus wind data product [20,22].

A detailed discussion about the optical architecture of the A2D can be found in [18,19]. Here, only the components that are important for this study are revealed. It is worth adding that the A2D was optimized for wind measurements but also provides the capability to measure temperature based on RB scattering. The laser consists of an injection-seeded, frequency-tripled, diode-pumped and pulsed Nd:YAG laser with an output energy of 60 mJ/pulse, a pulse repetition rate of 50 Hz, and a linewidth of 50 MHz (FWHM) at 354.9 nm (844.754 THz). A seed laser enables single frequency operation and tuning the laser frequency with high frequency stability (0.3 MHz RMS) over a range of 12 GHz, which is needed to sample the RB spectrum. The backscattered light is collected with a Cassegrain telescope with a 20 cm primary mirror diameter and directed to the optical receiver that consists of a field stop that limits the field of view to 100 μrad and several interferometers that are usually used for wind measurements. Here, only one of the two FPIs is used to sample the RB spectrum. The plates of the FPI are separated by 13.68 mm, leading to a free spectral range of 10.95 GHz, and the FWHM of the transmission curve is about 1.78 GHz. The light passing through the FPI is detected with an accumulation charge-coupled device.

Performing an accurate wind retrieval with the A2D requires instrument calibration measurements [18,23] that allow establishing the relationship between the Doppler frequency shift, and the corresponding response of the spectrometers. To determine this relationship, a frequency scan of the laser is carried out, thus simulating well-defined Doppler shifts of the radiation backscattered from the atmosphere. During the calibration, the contribution of the actual atmospheric wind along the line of sight of the instrument has to be eliminated. For this purpose, the calibration is carried out with nadir pointed lidar beams accomplished by flying curves at a roll angle of 20°, to compensate for the fixed off-nadir angle of the A2D instrument while assuming negligible vertical winds.

During one particular flight of NAWDEX, the A2D calibration method was adapted to an extended frequency range of 11 GHz such that RB spectra were measured with sufficient spectral coverage, thus allowing to determine an atmospheric temperature profile. On October 15, 2016, at 15:24 UTC, the Falcon took off from Keflavik airport heading towards the Vatnajākull glacier where one regular A2D calibration was performed. Due to clouds above the glacier, the aircraft moved farther north (65.1°N, 17.9°W) to perform another two A2D calibrations, followed by the temperature measurement (Fig. 1, magenta). The flight altitude was 10.97 km, and the measurement lasted from 18:00 UTC to 18:14 UTC. Afterwards, the Falcon returned to Keflavik airport and landed at 18:40 UTC. The corresponding flight track with the characteristic cycloidal flight pattern due to the drift of the aircraft with crosswind is shown in Fig. 1.

For the temperature measurement, the A2D laser frequency is changed in defined steps of 250 MHz over a frequency range of 11 GHz (at 354.9 nm). For each frequency step, one observation consists of the atmospheric returns from 630 pulses and takes 14 s. It needs an additional 4 s to change the laser frequency to the next step, a time during which no data are acquired. Thus, the entire sampling of the RB spectrum takes 14 min. The measured RB spectra for all altitudes normalized to unit area are shown in Fig. 2. The given altitudes indicate the center of the respective range bin, and the lowest valid measurement above the ground was at 1.84 km. The RB spectra at different altitudes look similar and are characterized by lower amplitude and larger width at low altitudes, which suggests higher temperatures in

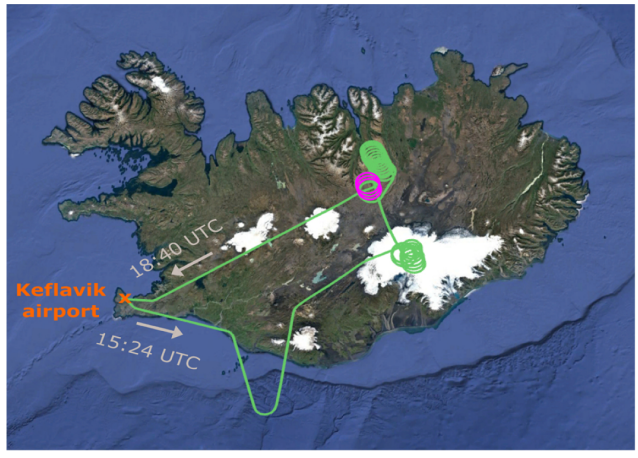

Fig. 1. Flight track of the aircraft on October 15, 2016, over Iceland (green). The area of the temperature measurement is indicated in magenta. Background image:© 2020 Google.

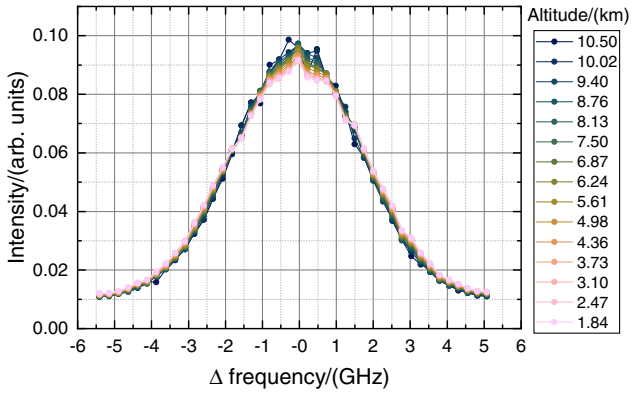

Fig. 2. RB spectra for different altitudes measured on October 15, 2016 (18:00 UTC to 18:14 UTC), normalized to unit area.

that region. To retrieve the actual temperature, the retrieval steps explained in Witschas *et al.* [6] are performed. In particular, the convolution of the FPI transmission curve, the spectral line shape of the laser, as well as the spectral distribution of the backscattered light is fitted in a least squares procedure to the measured spectra. Hence, not only an accurate RB line shape model but also an accurate treatment of the spectral features of the FPI is important as revealed by Witschas *et al.* [6]. The RB spectrum itself is well described by the Tenti S6 model [24,25], as demonstrated by several laboratory measurements [26–29] and atmospheric measurements [30]. To enable analytical fit procedures, a parameterized version of the Tenti S6 model according to Witschas [31,32] is used. Furthermore, in the presence of aerosols, particle scattering leads to an additional narrowband spectral component at the center frequency position, which is also considered in the fit routine.

Since the atmospheric pressure is not measured, it is taken from the U.S. standard atmosphere [33]. This is a justifiable approach, as simulations reveal that pressure uncertainties of 10 hPa cause a systematic error in the retrieved temperature of <0.1 K. The corresponding random error of the retrieved temperatures is calculated by means of a maximum likelihood estimator (MLE) method and considering Poisson noise only. The actual random error is likely to be larger due to the rather harsh and unstable conditions in the aircraft that may act on the laser frequency stability [34] and pointing direction, which in turn can slightly influence the actual transmission through the FPI. As shown by Hagen *et al.* [35], the standard deviation σ_w of the width w of a Gaussian profile can be estimated using an MLE according to $\sigma_w = w \cdot (2N)^{-1/2}$, where N is the total number of detected photo electrons. If the effect of Brillouin scattering is neglected, the RB spectrum has a Gaussian shape described by the Maxwell velocity distribution with a width of $w_\mathrm{m} = 2/\lambda \cdot (kT/m)^{1/2}$, where $\lambda = 354.9$ nm is the laser wavelength, $k = 1.38 \cdot 10^{-23}\,\mathrm{kg\,m^2\,s^{-2}\,K^{-1}}$ the Boltzmann constant, and $m = 4.798 \cdot 10^{-26}$ kg the average mass of one air molecule. Additionally, the FPI transmission curve can be approximated to follow a Gaussian shape with a width of $w_\mathrm{FPI} \approx 723$ MHz. Thus, the overall width w is given by $w = (w_\mathrm{m}^2 + w_\mathrm{FPI}^2)^{1/2}$. To convert σ_w from Hertz to Kelvin, the derivative $\partial w/\partial T$ is equalized with σ_w to finally get

$$\sigma_w = \frac{w_\mathrm{FPI}^2 \lambda^2 m}{2k\sqrt{2N}} + \frac{\sqrt{2}T}{\sqrt{N}} \approx \frac{80.84\,\mathrm{K}}{\sqrt{N}} + \frac{\sqrt{2}T}{\sqrt{N}}, \qquad (1)$$

where the first term is the contribution of the instrument function and thus independent of T, and the second term is the contribution of the spectrum of the scattered light. It is worth mentioning that for typical tropospheric temperatures (220 K to 320 K), the contribution of the measured spectrum to the random error [second term in Eq. (1)] is a factor of three to four larger than the one of the instrument function [first term in Eq. (1)]. For the measurement performed on October 15, 2016, the random error of the retrieved temperatures varies between 0.1 K and 0.4 K. From Eq. (1), it is also deduced that a random error below 1 K can be obtained with a quarter of the detected photons, meaning that both measurement time as well as the vertical bin size of the measurements can in principle be further reduced.

The retrieved temperatures are shown in Fig. 3 (left, red curve), while the corresponding random errors estimated from Eq. (1) are shown in Fig. 3 (left, error bars). The temperature profiles measured by a radiosonde at a distance of 250 km from the actual measurement location (65.1°N, 17.9°W) at 12:00 UTC is shown in green. The black curve represents the temperature obtained from the European Centre for Medium-Range Weather Forecasts (ECMWF) operational analysis that was spatially interpolated to the measurement location. The corresponding differences are plotted in the right panel.

The temperatures retrieved from the lidar measurements are in reasonable accordance with both the temperature profiles measured by the radiosonde and the one modeled by the ECMWF. The gray areas mark regions of invalid temperatures. Temperatures derived within the first 2.5 km from the instrument are affected by an incomplete telescope overlap and are thus considered to be unreliable. Though the laser is transmitted coaxially to the optical axis of the telescope, the backscattered light close to the instrument is obscured by the secondary mirror such that full overlap is reached about 3 km away from the instrument [36]. The measurement closest to the ground is likely to be affected by ground return, which considerably alters the backscatter spectrum and is hence also treated as invalid. The valid temperature values cause biases of less than ±2 K compared to radiosonde and the model. Further, the deviation to model temperatures exhibits an altitude dependency, i.e., the lidar yields a warm-bias for lower altitudes and a cold-bias for

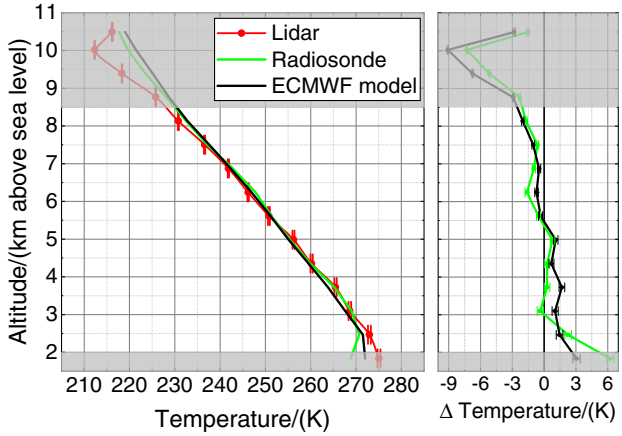

Fig. 3. Left: temperature profiles measured by the lidar (red) and radiosonde (green) as well as simulated ECMWF analysis (black). Right: temperature differences and error bars considering the random error of the lidar measurements [Eq. (1)]. The gray areas mark regions with invalid lidar measurements.

higher ones, a characteristic that was already observed from the ground-based measurements [6]. This behavior could be explained by an altitude-dependent illumination of the FPI, which means that the backscattered light from different altitudes has a different effective illumination angle, which in turn leads to a slightly different FPI transmission function. Consequently, a bias-free temperature retrieval could be implemented considering a range-dependent FPI transmission function. With the derivation of Eq. (1), it can be shown that a FWHM change of the FPI of 6.7 MHz changes the retrieved temperature by1 K.

In this Letter, it was demonstrated for the first time that tropospheric temperature profiles can be acquired during daytime from an airborne platform by means of lidar making use of RB scattering. The comparison with radiosonde and ECMWF model data reveals biases of smaller than ±2 K between 2 km and 8.5 km altitude. The corresponding random error varies between 0.1 K and 0.4 K.

To be less sensitive to varying atmospheric conditions during measurement, to be able to further shorten the measurement time, and to be more flexible in the post processing, it is suggested to use an imaging Fizeau interferometer with a multi-channel photomultiplier tube detector in the future [37]. Such a system makes no use of laser frequency or interferometer scanning procedures and is currently under development at DLR. First successful ground-based measurements have been performed, and first results were recently published [38]. In addition, it is foreseen to investigate the possibility of combining the suggested temperature lidar approach with a Raman lidar that can retrieve temperature more accurately in aerosol-rich or cloudy areas.

Funding. Deutsches Zentrum für Luft-und Raumfahrt (WindVal II); ESA (4000114053/15/NL/FF/gp); U.S. Naval Research Laboratory; EUFAR (project NAWDEX Influence).

Acknowledgment. We thank A. G. Straume-Lindner (ESA) for fruitful discussions in the beginning of our work related to atmospheric temperature measurements in the framework of ESA's Network Partnering Initiative. Additionally, we thank E. Nagel (DLR) for the prolonged technical support and the DLR pilots for sustaining to fly curves with the Falcon aircraft for several hours.

Disclosures. The authors declare no conflicts of interest.

Data Availability. Data underlying the results presented in this Letter are not publicly available at this time but may be obtained from the authors upon reasonable request.

REFERENCES

1. V. Wulfmeyer, R. M. Hardesty, D. D. Turner, A. Behrendt, M. P. Cadeddu, P. Di Girolamo, P. Schlüssel, J. Van Baelen, and F. Zus, Rev. Geophys. **53**, 819 (2015).
2. M. Alpers, R. Eixmann, C. Fricke-Begemann, M. Gerding, and J. Höffner, Atmos. Chem. Phys. **4**, 793 (2004).
3. A. Behrendt and J. Reichardt, Appl. Opt. **39**, 1372 (2000).
4. M. Radlach, A. Behrendt, and V. Wulfmeyer, Atmos. Chem. Phys. **8**, 159 (2008).
5. D. Hua, M. Uchida, and T. Kobayashi, Appl. Opt. **44**, 1315 (2005).
6. B. Witschas, C. Lemmerz, and O. Reitebuch, Opt. Lett. **39**, 1972 (2014).
7. C. She, R. Alvarez, II, L. Caldwell, and D. A. Krueger, Opt. Lett. **17**, 541 (1992).
8. J. W. Hair, L. M. Caldwell, D. A. Krueger, and C.-Y. She, Appl. Opt. **40**, 5280 (2001).
9. C.-Y. She, D. A. Krueger, Z.-A. Yan, and X. Hu, Opt. Express **29**, 4338 (2021).
10. R. A. Stillwell, S. M. Spuler, M. Hayman, K. S. Repasky, and C. E. Bunn, Opt. Express **28**, 71 (2020).
11. D. C. Fritts, R. B. Smith, M. J. Taylor, J. D. Doyle, S. D. Eckermann, A. Dörnbrack, M. Rapp, B. P. Williams, P.-D. Pautet, K. Bossert, N. R. Criddle, C. A. Reynolds, P. A. Reinecke, M. Uddstrom, M. J. Revell, R. Turner, B. Kaifler, J. S. Wagner, T. Mixa, C. G. Kruse, A. D. Nugent, C. D. Watson, S. Gisinger, S. M. Smith, R. S. Lieberman, B. Laughman, J. J. Moore, W. O. Brown, J. A. Haggerty, A. Rockwell, G. J. Stossmeister, S. F. Williams, G. Hernandez, D. J. Murphy, A. R. Klekociuk, I. M. Reid, and J. Ma, Bull. Am. Meteorol. Soc. **97**, 425 (2016).
12. M. Rapp, B. Kaifler, A. Dörnbrack, S. Gisinger, T. Mixa, R. Reichert, N. Kaifler, S. Knobloch, R. Eckert, N. Wildmann, A. Giez, L. Krasauskas, P. Preusse, M. Geldenhuys, M. Riese, W. Woiwode, F. Friedl-Vallon, B.-M. Sinnhuber, A. de la Torre, P. Alexander, J. L. Hormaechea, D. Janches, M. Garhammer, J. L. Chau, J. F. Conte, P. Hoor, and A. Engel, Bull. Am. Meteorol. Soc. **102**(4), E871 (2020).
13. W. S. Heaps and J. Burris, Appl. Opt. **35**, 7128 (1996).
14. J. Burris, T. McGee, W. Hoegy, L. Lait, L. Twigg, G. Sumnicht, W. Heaps, C. Hostetler, T. P. Bui, R. Neuber, and I. S. McDermid, J. Geophys. Res. Atmos. **107**, SOL29 (2002).
15. D. Wu, Z. Wang, P. Wechsler, N. Mahon, M. Deng, B. Glover, M. Burkhart, W. Kuestner, and B. Heesen, Opt. Express **24**, A1210 (2016).
16. A. Rekhy, A. Gerakis, D. Feng, M. N. Shneider, A. Dogariu, and R. B. Miles, in *AIAA Aviation 2019 Forum* (2019), p. 3286.
17. A. Schäfler, G. Craig, H. Wernli, P. Arbogast, J. D. Doyle, R. McTaggart-Cowan, J. Methven, G. Rivière, F. Ament, M. Boettcher, M. Bramberger, Q. Cazenave, R. Cotton, S. Crewell, J. Delanoë, A. Dörnbrack, A. Ehrlich, F. Ewald, A. Fix, C. Grams, S. Gray, H. Grob, S. Gross, M. Hagen, B. Harvey, L. Hirsch, M. Jacob, T. Kölling, H. Konow, C. Lemmerz, O. Lux, L. Magnusson, B. Mayer, M. Mech, R. W. Moore, J. Pelon, J. Quinting, S. Rahm, M. Rapp, M. Rautenhaus, O. Reitebuch, C. Reynolds, H. Sodemann, T. Spengler, G. Vaughan, M. Wendisch, M. Wirth, B. Witschas, K. Wolf, and T. Zinner, Bull. Am. Meteorol. Soc. **99**(8), 1607 (2018).
18. O. Lux, C. Lemmerz, F. Weiler, U. Marksteiner, B. Witschas, S. Rahm, A. Schäfler, and O. Reitebuch, Atmos. Meas. Tech. **11**, 3297 (2018).
19. O. Reitebuch, C. Lemmerz, E. Nagel, U. Paffrath, Y. Durand, M. Endemann, F. Fabre, and M. Chaloupy, J. Atmos. Ocean. Technol. **26**, 2501 (2009).
20. O. Lux, C. Lemmerz, F. Weiler, U. Marksteiner, B. Witschas, S. Rahm, A. Geiß, and O. Reitebuch, Atmos. Meas. Tech. **13**, 2075 (2020).
21. B. Witschas, S. Rahm, A. Dörnbrack, J. Wagner, and M. Rapp, J. Atmos. Ocean. Technol. **34**, 1371 (2017).
22. B. Witschas, C. Lemmerz, A. Geiß, O. Lux, U. Marksteiner, S. Rahm, O. Reitebuch, and F. Weiler, Atmos. Meas. Tech. **13**, 2381 (2020).
23. U. Marksteiner, C. Lemmerz, O. Lux, S. Rahm, A. Schäfler, B. Witschas, and O. Reitebuch, Remote Sens. **10**, 2056 (2018).
24. C. Boley, R. Desai, and G. Tenti, Can. J. Phys. **50**, 2158 (1972).
25. G. Tenti, C. D. Boley, and R. C. Desai, Can. J. Phys. **52**, 285 (1974).
26. B. Witschas, M. O. Vieitez, E.-J. van Duijn, O. Reitebuch, W. van de Water, and W. Ubachs, Appl. Opt. **49**, 4217 (2010).
27. M. Vieitez, E. van Duijn, W. Ubachs, B. Witschas, A. Meijer, A. de Wijn, N. Dam, and W. van de Water, Phys. Rev. A **82**, 43836 (2010).
28. B. Witschas, Z. Gu, and W. Ubachs, Opt. Express **22**, 29655 (2014).
29. Z. Gu, B. Witschas, W. van de Water, and W. Ubachs, Appl. Opt. **52**, 4640 (2013).
30. B. Witschas, C. Lemmerz, and O. Reitebuch, Appl. Opt. **51**, 6207 (2012).
31. B. Witschas, Appl. Opt. **50**, 267 (2011).
32. B. Witschas, Appl. Opt. **50**, 5758 (2011).
33. *US Standard Atmosphere* (US Government Printing Office, 1976).
34. C. Lemmerz, O. Lux, O. Reitebuch, B. Witschas, and C. Wührer, Appl. Opt. **56**, 9057 (2017).
35. N. Hagen, M. Kupinski, and E. Dereniak, Appl. Opt. **46**, 5374 (2007).
36. U. Paffrath, "Performance assessment of the Aeolus Doppler wind lidar prototype," Ph.d. thesis (Technical University of Munich, 2006).
37. J. Xu, B. Witschas, K. Liang, Y. Wang, and W. Ubachs, in *EPJ Web of Conferences* (2019) 07004.
38. J. Xu, B. Witschas, P. G. Kabelka, and K. Liang, Opt. Lett. **46**, 3320 (2021).